# Probing the Electronic Structure of the Di-Iron Subsite of [Fe]-Hydrogenase: A Photoelectron Spectroscopic Study of Fe(I)−Fe(I) Model Complexes

**Xin Yang,[†] Mathieu Razavet,[‡] Xue-Bin Wang,[†] Christopher J. Pickett,*[,‡] and Lai-Sheng Wang*[,†]**

*Contribution from the Department of Physics, Washington State University, 2710 University Drive, Richland, Washington 99352, W.R. Wiley Environmental Molecular Sciences Laboratory, MS K8-88, P.O. Box 999, Pacific Northwest National Laboratory, Richland, Washington 99352, and Department of Biological Chemistry, John Innes Centre, Norwich NR4 7UH, U.K.*

*Received: February 20, 2003; In Final Form: April 17, 2003*

The electronic structures of a series of Fe(I)−Fe(I) model complexes of the di-iron subsite of [Fe]-hydrogenase, $[(\mu\text{-PDT})Fe_2(CO)_4(CN)_2]^{2-}$ (**I**), $[Fe_2(CO)_4\{MeSCH_2C(Me)(CH_2S)_2\}(CN)_2]^{2-}$ (**II**), $[Fe_2(CO)_4\{PhCH_2SCH_2C(Me)(CH_2S)_2\}(CN)_2]^{2-}$ (**III**), $[Fe_2(CO)_4\{PhCH_2SCH_2C(Me)\ (CH_2S)_2\}(CN)]^-$ (**IV**), and $[Fe_2(CO)_4\{MeSCH_2C(Me)(CH_2S)_2\}(CN)]^-$ (**V**), were investigated in the gas phase using photodetachment photoelectron spectroscopy. The adiabatic electron detachment energy (ADE) of each species and the intramolecular Coulomb repulsion for the doubly charged species were obtained. The ADEs correspond to the intrinsic redox potentials (in vacuo) of reactions involving the Fe(I)−Fe(I)/Fe(I)−Fe(II) couples in these compounds. The photoelectron spectra were understood and qualitatively assigned by comparing with that of $Fe_2(CO)_6S_2$, which has been well studied previously and exhibits similar valence spectral features as **I**−**V**. A "normal level scheme" is suggested for the electronic structure of these low spin di-iron compounds, in which all occupied 3d levels lie above all occupied ligand levels. We also observed subtle differences in the electronic structures of the five di-iron complexes due to the slightly different ligand environments.

## 1. Introduction

All-iron hydrogenases are one of two major classes of metalloproteins catalyzing the reversible activation of molecular hydrogen according to the reaction, $H_2 \leftrightarrow 2H^+ + 2e^-$. In living systems, the [Fe]-hydrogenases are mainly used to reduce protons to $H_2$.[1−4] Various spectroscopic methods have been applied to investigate their structures, and an unusual Fe−S cluster, called H-cluster, has been proposed to be the site of hydrogen activation.[1] FTIR[5−7] and X-ray structure[8,9] studies show that the H-cluster from different organisms are essentially the same and consist of a di-iron subcluster linked by a cysteine thiolate to a [4Fe4S] cluster (Figure 1). Each iron of the di-iron subclusters is coordinated by a terminal CO, a bridging CO and a CN ligand; the two Fe atoms of the subsite share two bridging sulfur ligands of a propanedithiolate or azapropanedithiolate unit.[10−12]

The H-cluster has been found to possess three oxidation states during the catalytical cycle. The fully oxidized inactive H-cluster and the completely reduced H-cluster are EPR silent, whereas the partially oxidized active H-cluster is paramagnetic ($S = 1/2$).[7] On the basis of Mössbauer, EPR, and ENDOR spectroscopic studies, Popescu and Münck suggested that the [4Fe4S] subcluster carries a 2+ charge in both oxidized and reduced forms of the H-cluster.[13] Thus, the oxidation states of the di-iron subcluster involved in the catalytic cycle can be either Fe(II)−Fe(II) ↔ Fe(II)−Fe(III) ↔ Fe(III)−Fe(III) or Fe(I)−Fe(I) ↔ Fe(I)−Fe(II) ↔ Fe(II)−Fe(II).

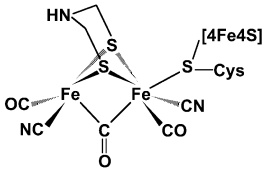


**Figure 1.** Schematic structure of the H-cluster in [Fe]-hydrogenase.

Experimental support for a paramagnetic Fe(I)−Fe(II) state comes from $^{13}CO$ labeling studies on the H-center of hydrogenase by DeLacey et al.,[11] who have argued on the basis of the $\nu$(CO) frequencies associated with the distal paramagnetic Fe atom that this center must be Fe(I). Some Fe(I)−Fe(I) model complexes, such as $[(\mu\text{-PDT})Fe_2(CO)_4(CN)_2]^{2-}$ (PDT = $SCH_2CH_2CH_2S$), have been synthesized and characterized recently, which are stable and structurally similar to the di-iron center of the H-cluster in its CO-inhibited form.[14−22] Furthermore, it has been reported that a transient Fe(I)−Fe(II) di-cyanide species generated by one-electron oxidation of an Fe(I)−Fe(I) complex shows $\nu(CO)_{terminal}$ and $\nu(CO)_{bridge}$ at frequencies very close to those of the oxidized CO-inhibited form of the H-cluster.[16]

Using density functional theory (DFT), Cao and Hall have calculated the structures of the di-iron subcluster in the H-cluster.[23] By comparing the calculated $CN^-$ and $CO^-$ vibrational frequencies with the observed bands of *D. vulgaris* [Fe]-hydrogenase, they proposed that the oxidized inactive enzyme should be an Fe(II)−Fe(II) species, whereas an Fe(I)−Fe(II) species and an Fe(I)−Fe(I) species are responsible for the active EPR-detectable state and the fully reduced EPR-silent state, respectively. Their results preclude the presence of Fe(III)−Fe(II) or Fe(III)−Fe(III) states in the catalytic cycle,

* To whom correspondence should be addressed. E-mail: chris.pickett@bbsrc.ac.uk and ls.wang@pnl.gov.
[†] Washington State University and Pacific Northwest National Laboratory.
[‡] John Innes Centre.

10.1021/jp034432i CCC: $25.00 
Published on Web 05/16/2003

and these calculations have been recently confirmed by Liu and Hu.[24]

Extensive theoretical studies have been focused on the electronic structures of Fe−S clusters.[25−28] In these clusters, each Fe possesses a high-spin state, and an "inverted level scheme" pattern is obtained for their molecular orbital (MO) energy levels, in which strong exchange interactions split the Fe 3d levels into a set of spin-up ($\alpha$) and a set of spin-down ($\beta$) levels with the primarily ligand-based levels in between.[25−27] This "inverted level scheme" has been shown to apply to Fe−S complexes[27] with one to four Fe and has been investigated experimentally.[29−31] In the di-iron active site of the [Fe]-hydrogenase, each iron coordinates with both strong-field ligands (CO, $CN^-$) and weak-field ligands (−S) (Figure 1). In addition, the Fe−Fe distance is shorter and there exist weak Fe−Fe bonding interactions. Therefore, the electronic structure of the di-iron site of the [Fe]-hydrogenase is expected to be more complicated. Most previous theoretical studies have focused on the vibrational properties and catalytic mechanisms,[23,24,32] and there has been very limited effort on the electronic structures of the di-iron subcluster of the [Fe]-hydogenases.[24] However, understanding the detailed electronic structure of the 2Fe subcluster is likely to be critical in elucidating the catalytic mechanisms of the H-cluster.

Gas-phase photodetachment photoelectron spectroscopy (PES) is an excellent tool to study the electronic structure and chemical bonding of isolated molecules or inorganic complexes without the perturbation in the condensed phase. We have developed an experimental technique, which couples electrospray ionization (ESI) with a magnetic-bottle photoelectron spectrometer.[33] ESI is a versatile technique, allowing ionic species in solution samples to be transported into the gas phase. Our recent research has shown that the new ESI−PES technique is ideal for investigating multiply charged anions in the gas phase, as well as anionic metal complexes commonly present in solution.[34,35] Using this technique, we have carried out a preliminary study of a series of [1Fe]-complex anions involved in the $Fe^{2+}-Fe^{3+}$ redox couple,[36] with emphasis on the determination of the intramolecular reorganization energies. PES studies on a series of [1Fe] and [4Fe] complexes have been carried out recently.[37,38] The spectral patterns of these complexes agreed well with spin polarized DFT calculations, suggesting that the "inverted level scheme" is a general feature of the electronic structures of the Fe−S complexes.

In the current paper, we report gas-phase PES studies of five Fe(I)−Fe(I) model complexes of the 2Fe sub-site in the H-cluster of the [Fe]-hydrogenase, $[(\mu\text{-PDT})Fe_2(CO)_4(CN)_2]^{2-}$ (**I**), $[Fe_2(CO)_4\{MeSCH_2C(Me)(CH_2S)_2\}(CN)_2]^{2-}$ (**II**), $[Fe_2(CO)_4\{PhCH_2SCH_2C(Me)(CH_2S)_2\}(CN)_2]^{2-}$ (**III**), $[Fe_2(CO)_4\{PhCH_2SCH_2C(Me)(CH_2S)_2\}(CN)]^-$ (**IV**), $[Fe_2(CO)_4\{MeSCH_2C(Me)(CH_2S)_2\}(CN)]^-$ (**V**). The schematic molecular structures for **I**−**V** are shown in Figure 2. PES spectra for each anion were taken at three photon energies: 266 (4.661), 193 (6.424), and 157 nm (7.866 eV). Spectral features were assigned on the basis of previous theoretical works and past experience with related molecules. A "normal level scheme" is found for the molecular orbitals of these low spin di-iron compounds, in which all occupied metal 3d levels lie above the ligand levels. The adiabatic electron detachment energy (ADE) of each species and the intramolecular coulomb repulsion for each dianion were determined.

## 2. Experimental Section

Details of the ESI−PES apparatus were published elsewhere.[33] Only a brief description of the experimental procedure is given here. To produce the desired anions, we used $10^{-3}$ molar solutions of their $[NEt_4]^+$ or $[K^+18\text{-crown-6}]$ salts in pure acetonitrile. Details of the synthesis and characterization of these compounds have been reported.[14−17] Sample solutions were sprayed through a 0.01 mm diameter syringe needle biased at −2.2 kV in a pure $N_2$ atmosphere. Negatively charged ions emerging from a desolvation capillary were guided by a radio frequency-only quadrupole ion-guide into an ion trap, where the anions were accumulated for 0.1 s before being pushed into the extraction zone of a time-of-flight mass spectrometer.

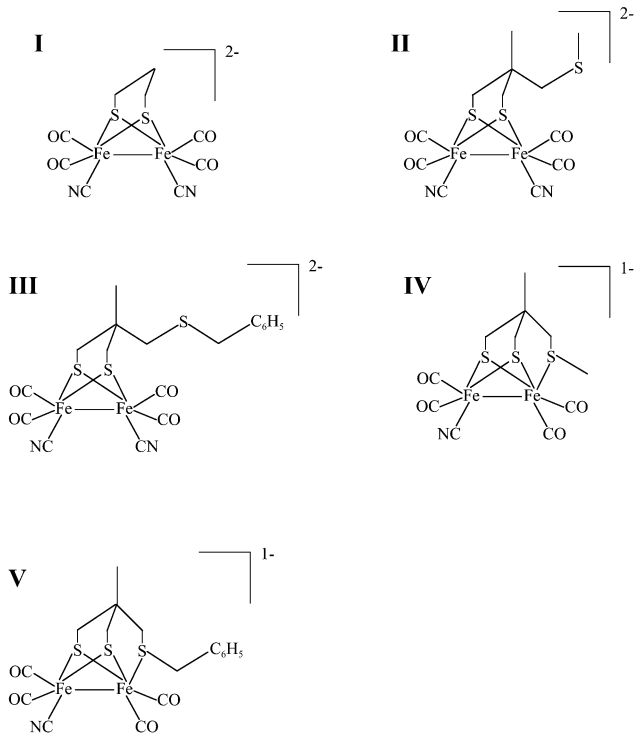


**Figure 2.** Schematic molecular structures of the five model complexes: **I**, $[(\mu\text{-PDT})Fe_2(CO)_4(CN)_2]^{2-}$, **II,** $[Fe_2(CO)_4\{MeSCH_2C(Me)(CH_2S)_2\}(CN)_2]^{2-}$; **III**, $[Fe_2(CO)_4\{PhCH_2SCH_2C(Me)(CH_2S)_2\}(CN)_2]^{2-}$; **IV**, $[Fe_2(CO)_4\{PhCH_2SCH_2C(Me)(CH_2S)_2\}(CN)]^-$; **V**, $[Fe_2(CO)_4\{MeSCH_2C(Me)(CH_2S)_2\}(CN)]^-$.

In the PES experiment, the anions of interest were mass-selected and decelerated before being intercepted by a laser beam in the detachment zone of the magnetic-bottle photoelectron analyzer. For the current study, three photon energies were used for detachment: 266 nm from a Q-switched Nd:YAG laser and 193 and 157 nm from an excimer laser. Photoelectrons were collected at nearly 100% efficiency by the magnetic bottle and analyzed in a 4-m long time-of-flight tube. Photoelectron time-of-flight spectra were collected and then converted to kinetic energy spectra, calibrated by the known spectra of $I^-$ and $O^-$. The binding energy spectra were obtained by subtracting the kinetic energy spectra from the corresponding photon energies. The energy resolution ($\Delta E/E$) was about 2%, i.e., 10 meV for ~0.5 eV electrons, as measured from the spectrum of $I^-$ at 355 nm.

## 3. Results

**3.1. Photoelectron Spectra at 157 nm.** Figure 3 shows the PES spectra of all of the five anions at 157 nm. The overall spectral patterns of the three doubly charged anions **I**−**III** are very similar. In the spectrum of **I** (Figure 3a), four bands were observed between 0 and 6 eV, as well as a sharp peak centered at 7.3 eV (D). Bands X and A were very broad, whereas band

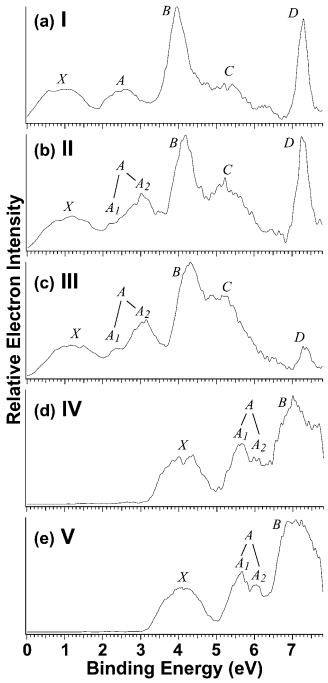


**Figure 3.** Photoelectron spectra of **I**−**V** at 157 nm (7.866 eV).

B was relatively sharp and intense. Band C was also broad and appeared to be overlapped with band B. In the spectrum of **II** (Figure 3b), bands X, B, and D are nearly identical to those observed in the spectrum of **I**. However, bands A and C showed some differences: band A of **II** was more complicated and appeared to contain two components ($A_1$, $A_2$); the band C of **II** was more intense compared to that of **I**. The spectrum of **III** (Figure 3c) is nearly identical to that of **II**: the $A_1$ and $A_2$ components of the A band were even better resolved in **III** and band C was even more intense. However, the intensity of band D in **III** decreased dramatically relative to that in **I** and **II**. From **I** to **III**, all of the spectral features (X, A−C) shift slightly to higher binding energies, except for band *D*, which appeared in the same binding energy in all three spectra. As we will show below, band D in **I**−**III** could not be due to direct photodetachment transitions because of the repulsive coulomb barrier (RCB) present in the doubly charged anions.

The two singly charged anions have much higher binding energies because of the lack of intramolecular coulomb repulsion that is present in the three doubly charged anions. The photoelectron spectra of the two singly charged anions **IV** (Figure 3d) and **V** (Figure 3e) are nearly identical to each other. The overall spectral patterns of **IV** and **V** are similar to those in **I**−**III**, in particular, the X band is almost identical to that in **I**−**III**. The shapes of the A and B bands are different from those in **I**−**III**. The A band also seemed to contain two components, but the $A_1$ subband was more intense in **IV** and **V** than in **II** and **III**. The B band in **IV** and **V** was broader and less intense compared to that in **I**−**III**. It was expected that a similar C band might exist in the spectra of **IV** and **V** at higher binding energies beyond the 157 nm photon energy.

**3.2. Photon-Energy-Dependent Studies.** Photoelectron spectra of **I**−**III** at three photon energies are shown in Figures 4−6, respectively. Spectral features were better resolved at the lower detachment photon energies. In the 193 nm spectra, the X bands in all three species were resolved into two subbands ($X_1$ and $X_2$). The A band was also resolved more clearly into two components ($A_1$ and $A_2$), especially in **II** and **III**. In **I**, the $A_1$ subband, which was not resolved in the 157 nm spectrum (Figure 3a), appeared as a shoulder in the 193 nm spectrum (Figure 4b). Band C was cut off in the 193 nm spectra of **I** and **II** because of the repulsive coulomb barrier, which will be discussed below. In the 193 nm spectrum of **III** (Figure 6b), the B band became broader because of partial contributions from the band C, which was not completely cut off. The 266 nm spectra showed that the X band in all three species in fact contained many unresolved and closely spaced spectral features. The B band was completely cut off by the RCB, whereas the A band became very weak in the 266 nm spectra, again due to the RCB. We also obtained the spectra of the two singly charged anions (**IV** and **V**) at the lower photon energies (not shown). The X band in **IV** and **V** was also shown to have two subbands ($X_1$ and $X_2$), which were already discernible in the 193 nm spectrum of **IV** (Figure 3d).

The adiabatic detachment energies of the threshold peaks of each complex and the vertical detachment energies (VDEs) of

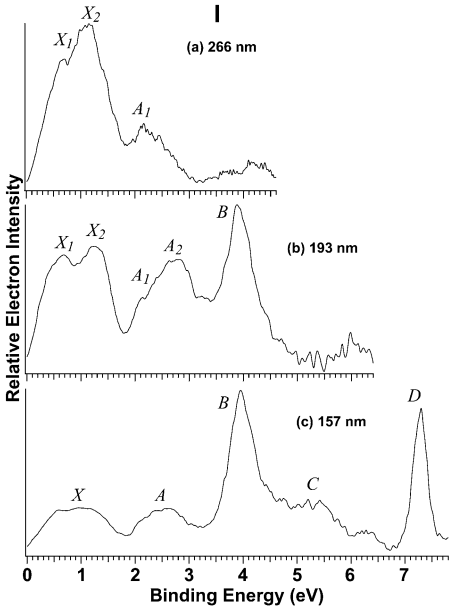


**Figure 4.** Photoelectron spectra of **I** at (a) 266 (4.661 eV), (b) 193 (6.424 eV), and (c) 157 nm.

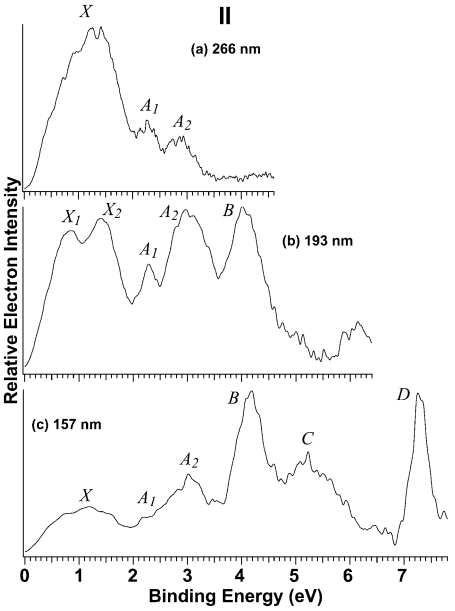


**Figure 5.** Photoelectron spectra of **II** at (a) 266, (b) 193, and (c) 157 nm.

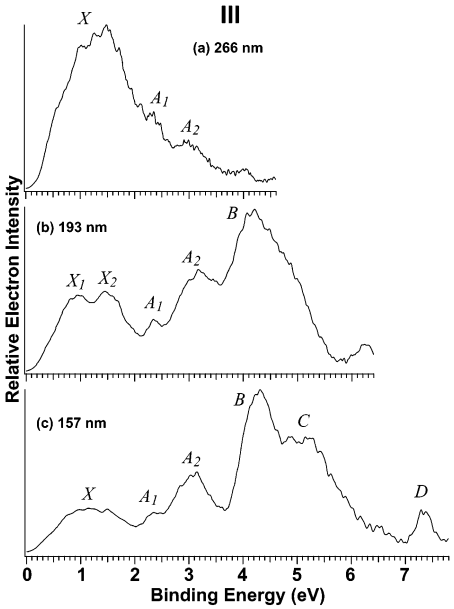


**Figure 6.** Photoelectron spectra of **III** at (a) 266, (b) 193, and (c) 157 nm.

all observed features are listed in Table 1. The ADEs represent the electron affinities of the neutral species for **IV** and **V** or the second electron affinities in the cases of **I**−**III**. They were measured by drawing a straight line along the leading edge of the threshold band and then adding a constant to the intersection with the binding energy axis to take into account the finite resolution and a thermal broadening. The ADEs were determined from the 266 nm spectra for each complex because of the better resolution at the lower photon energy. The VDE of each peak was measured straightforwardly from the peak maximum. However, because the PES spectra contained many unresolved and closely spaced detachment transitions, the VDEs in most cases should be considered as nominal numbers.

### 4. Spectral Assignments and Discussion

The PES features shown in Figures 3−6 represent transitions from the ground state of the dianions (**I**−**III**) or singly charged anions (**IV**, **V**) to the ground and excited states of the corresponding singly charged anions or neutral molecules. Within the single-particle approximation (Koopmans' theorem), the PES features can be viewed as removing electrons from the occupied molecular orbitals of the parent anions. Therefore, unlike other various experimental methods based on electronic transitions from occupied MOs to empty or partially occupied MOs, PES provides a direct map of the occupied MOs. Furthermore, for anions involved in electron transfer reactions (such as the di-iron active center in [Fe]-hydrogenase), PES data directly yield the intrinsic oxidation energy and intramolecular reorganization energy in the gas phase because photodetachment is equivalent to an oxidation process.[36] In the following, we will first discuss the repulsive coulomb barrier and the electrostatic interactions in the three doubly charged anions. We will then discuss the electronic structure and the PES data of **I**−**V** through comparison with a series of analogous and well-known inorganic di-iron metal complexes.

**4.1. Repulsive Coulomb Barrier and the Intramolecular Coulomb Repulsion in I**−**III.** The disappearance of the high binding energy features in the lower photon energy spectra of **I**−**III** (Figures 4−6) is a direct consequence of the repulsion coulomb barrier,[34,35,39] which exists universally in multiply charged anions because of the intramolecular coulomb repulsion and prevents slow electrons from being emitted. The RCB effects were seen most clearly by comparing the PES data at a lower photon energy to that at a higher photon energy. For example, the C band was cut off in all the 193 nm spectra of **I**−**III**, whereas the B band was completely cut off in all of the 266 nm spectra of **I**−**III**. From the spectral cutoff of the photon-energy-dependent spectra, we could estimate the RCB heights. The B band was relatively sharp and provided the ideal spectral feature to determine the barrier heights. The B band of **I** has a VDE of 3.96 eV, as measured from the 157 nm spectrum (Figure 4c). However, we note that the VDE of the B band is shifted slightly to a lower value in the 193 nm spectrum (Figure 4b). Furthermore, the intensity of the B band relative to that of the X and A bands was decreased in the 193 nm. Both of these observations suggested that the 193 nm photon was near or slightly below the RCB of the B band,[40] yielding approximately a barrier height of 2.5 eV (6.424−3.96 eV). This means that the spectral cutoff would be around 2.2 eV (4.661−2.5 eV) in the 266 nm spectrum. This was exactly the case as seen in Figure 4a, where the $A_2$ subband was completely cut off whereas the $A_1$ subband (VDE = 2.13 eV, Table 1) was not cut off. In fact, the 266 nm photon was right near the RCB top of the detachment transition to the $A_1$ subband. Using the same procedure and the data in Figures 5 and 6, we estimated the RCB heights to be 2.3 and 2.1 eV for **II** and **III**, respectively.

As shown previously,[41] the RCB is equivalent to the intramolecular coulomb repulsion derived from the excess charges. It is surprising that the RCB in **I**−**III** is not the same, because the three anions have the same coordination environment. The only difference among them is the distal side chains of the dithiolate ligands (Figure 2). The trend of the intramolecular coulomb repulsion from **I** to **III** is consistent with their ADE trend: the decreasing coulomb repulsion from **I** to **III** leads to the increase of ADE in the same direction. This observation indicates that the excess charges are also delocalized to a small degree to the distal ligands. This seems to be happening only for the multiply charged anions, because the ADEs of the two singly charged anions are identical within our experimental accuracy, despite the difference in the bound thioether ligands. We generally assumed that the gas phase conformations of **I**−**V** are similar to those in solutions as given in Figure 2. However, there is a slight possibility that in the gas phase the S from the distal thioether in **II** and **III** may coordinate to the proximal Fe, causing one CO from the proximal Fe to bridge both Fe. In solution, a bridged precursor to **II** and **III** is observed.[17] Although the bridged confirmation for **II** and **III** would readily explain their higher ADEs compared to that of **I**, a much stronger stabilization might have been expected.

The sharp peak (D) centered at 7.3 eV in the 157 nm spectra of **I**−**III** (Figure 3) was unexpected because it occurred in the RCB cutoff regime. As discussed above, the three dianions possess RCBs of 2.5, 2.3, and 2.1 eV, respectively, implying that electrons with kinetic energies less than these values would not be emitted, except through tunneling.[40] This caused the cutoff at the high binding energy side in the PES spectra at lower photon energies. However, the same cutoff applies in the 157 nm spectra. The origin of band D could be due to several processes: (1) detachment of singly charged anions from a two-photon event (i.e., $X^{2-} + h\nu \rightarrow X^- + e^-$; then $X^- + h\nu \rightarrow X + e^-$); (2) resonant tunneling due to production of a highly excited dianion upon resonant absorption of a 157 nm photon;[42] (3) thermionic emissions due to production of a "super" hot dianion if the absorbed photon in (2) is thermalized. We can

**TABLE 1: Measured Adiabatic Detachment Energies (ADE) for the Threshold Features and Vertical Detachment Energies (VDE) of All of the Observed Features for I−V[a]**

| | | VDE | | | | | |
|---|---|---|---|---|---|---|---|
| | ADE | $X_1$ | $X_2$ | $A_1$ | $A_2$ | B | C |
| **8.0qI** | 0.15 (10) | 0.67 (10) | 1.24 (10) | 2.13 (5) | ∼2.7 | 3.96 (8) | 4.5∼6 |
| **II** | 0.25 (10) | 0.84 (10) | 1.41 (10) | 2.29(8) | 2.96 (10) | 4.18 (8) | 4.8∼6 |
| **III** | 0.35 (10) | 0.95 (10) | 1.48 (10) | 2.35 (8) | 3.18 (8) | 4.32 (8) | 4.7∼6 |
| **IV** | 3.30 (10) | 3.9 (1) | ∼4.3 | 5.65 (8) | 6.04 (8) | 7.00 (10) | |
| **V** | 3.30 (8) | 3.86 (8) | ∼4.3 | 5.65 (8) | 6.04 (8) | 7.05 (10) | |

[a] All energies are in eV. The numbers in the parentheses represent the uncertainties in the last digits.

rule out (1) easily because the binding energy of 7.3 eV seemed to be too high and the peak was too sharp compared to the spectra of the singly charged **IV** and **V**. We have observed similar phenomena in a previous PES study of $Ru_6C(CO)_n^{2-}$ ($n$ = 9, 10) and attributed them to the thermionic emission tunneling through the RCB.[43] In the $Ru_6C(CO)_n^{2-}$ cases, we observed the sharp peak in the RCB forbidden region at different photon energies, suggesting that it was indeed due to process (3). As seen in Figures 4−6, the sharp peaks did not appear in the lower photon energy spectra. This could be due to the fact that there was no resonant absorption other than the 157 nm photon. In any case, we could not definitively assign the 7.3 eV peak, which could be due to either or both processes (2) and (3).

**4.2. Electronic Structures of $Fe_2(CO)_6S_2$-Type Complexes.** Although the structures of the di-iron active site of the [Fe]-hydrogenase were determined only recently, a group of ligand bridged di-iron hexacarbonyl complexes [$Fe_2(CO)_6S_2$] with similar structures had been synthesized and characterized since the 1960s.[44−46] In these molecules, each iron atom is coordinated with three terminal CO, and the two iron atoms are bridged by the two −S ligands, which can be the simple $S_2$ unit or two −SR ligands. Extensive theoretical and experimental investigations are available in the literature concerning the electronic structure and chemical bonding of the sulfur bridged species,[47−50] which are directly relevant to the model complexes in the present work.

Teo et al. first performed an extensive molecular orbital study on a series of $Fe_2(CO)_6X_2$ complexes.[47] For $Fe_2(CO)_6S_2$ and $Fe_2(CO)_6(SCH_3)_2$, the upper filled MOs can be divided into three sets of levels, as schematically shown in Figure 7. The first set consists of seven completely filled MO levels with mainly iron 3d character, including the HOMO ($5a_1$) which is an Fe−Fe bonding orbital. The LUMO is mainly an Fe−Fe antibonding orbital for $Fe_2(CO)_6(SCH_3)_2$ and an S−S antibonding orbital for $Fe_2(CO)_6S_2$. The second set of MOs ($1a_2$ and $1b_1$) is well separated from the seven 3d levels and mainly of Fe−S bonding character. Below these levels lies the third set of levels, which are primarily S lone pairs. The MOs derived from the terminal CO ligands ($5\sigma$ and $1\pi$) are below the S lone pairs. This is called a "normal level scheme", in that, all of the Fe 3d levels are above the occupied ligand levels.

The valence photoelectron spectra of $Fe_2(CO)_6S_2$ were measured in the gas phase[48,50] and confirmed the basic features of the MO scheme shown in Figure 7. Figure 8 reproduces the Ne(I) and He(I) PES spectra of $Fe_2(CO)_6S_2$ by Anderson et al.,[48] who assigned the five observed bands using several theoretical models. The bands 1−3 were assigned to correspond to the three sets of MOs as shown in Figure 7; bands 4 and 5 are assigned to derive from mainly the CO $1\pi$ and $5\sigma$, respectively. We will tentatively assign the PES data of **I**−**V** on the basis of the PES spectra and MO diagram of $Fe_2(CO)_6S_2$.

**4.3. Spectral Assignments of I by Comparison With That of $Fe_2(CO)_6S_2$.** The molecular structures of our analogues of the di-iron subsite of the H-cluster are very similar to $Fe_2(CO)_6S_2$ and $Fe_2(CO)_6(SCH_3)_2$. In fact, they were all synthesized by the cyanation of these carbonyl precursors.[14−20] The $CN^-$ ligand is isoelectronic to CO. Thus, the coordination environments and the oxidation state of Fe in **I**−**III** are similar to $Fe_2(CO)_6S_2$ or $Fe_2(CO)_6(SCH_3)_2$: the two excess charges in **I**−**III** are due to the charges carried by the $CN^-$ ligands. It is reasonable to believe that they should all have similar electronic structures. Indeed, we note that the PES spectra of **I**−**III** are rather similar to that of $Fe_2(CO)_6S_2$, as shown in Figure 8, where the 157 nm spectrum of **I** is plotted in the same energy scale as those of $Fe_2(CO)_6S_2$.

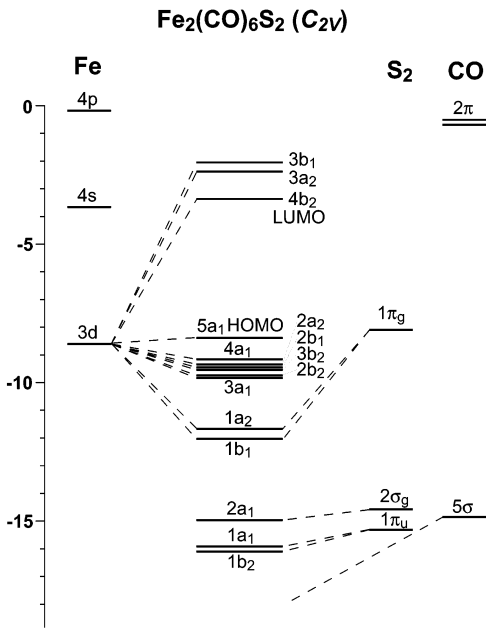


**Figure 7.** Schematic molecular orbital diagram of $Fe_2(CO)_6S_2$ from ref 47.

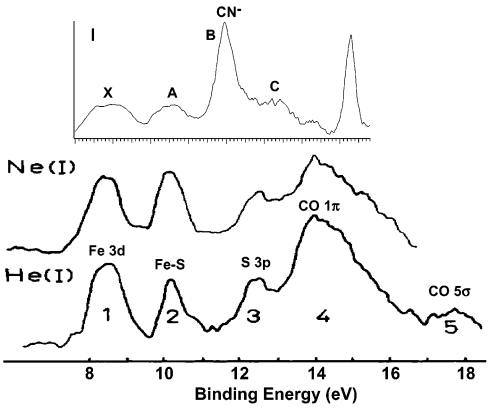


**Figure 8.** Comparison of the 157 nm spectrum of **I** to those of $Fe_2(CO)_6S_2$ at Ne(**I**) and He(**I**) radiations. The $Fe_2(CO)_6S_2$ spectra are from ref 48.

The bands X and A are nearly identical to the bands 1 and 2 of $Fe_2(CO)_6S_2$. Accordingly, we assign band X to be due to detachment from Fe 3d-derived orbitals, analogous to the top seven orbitals in the MO diagram of $Fe_2(CO)_6S_2$ (Figure 7). The fine features resolved in the lower photon energy spectra of **I** (Figure 4) should be due to the splitting of the Fe 3d orbitals. The band A of **I** is then due to detachment from the Fe−S bonding orbitals. The intense and sharp band B of **I** does not have a counterpart in the spectra of $Fe_2(CO)_6S_2$. This band is assigned to be from detachment from the $\pi$ orbitals of the $CN^-$ ligands. Because of its negative charge, the binding energy of $CN^-$ is expected to be lower than that of the CO ligands.[51] By comparing the spectra of **I** and $Fe_2(CO)_6S_2$, we note that the band C of **I** should contain the counterpart of band 3 of $Fe_2(CO)_6S_2$, i.e., the ionization from S lone pairs, and partially ionization of CO $\sigma$ orbitals on the higher binding energy side which was cut off by the RCB.

**4.4. Spectral Assignments of II and III.** Following the qualitative assignments of the spectral features of **I**, the assignments of the spectral features of **II** and **III** are straightforward. The X, A, and B bands of **II** and **III** are similar to those of **I** and should again be due to detachment from the Fe 3d, Fe−S bonding, and $CN^-$ $\pi$ orbitals, respectively. The splitting of the A band in **II** and **III** is slightly different from that in **I**. The $A_1$ and $A_2$ subbands in **II** and **III** are well separated, whereas they overlap in **I**. In addition, the $A_2$ subband in **II** and **III** appeared to be relatively more intense. These observations suggest that the S atom on the distal ligand in **II** and **III** (Figure 2) may contribute to the $A_2$ subband. Figure 3 shows that the relative intensity of the C band increases from **I** to **II** to **III**, implying that the distal S also contribute to the C band in **II** and **III**. In addition, the intense C band of **III** should also have contributions from the phenyl $\pi$ orbitals. Ionization of the phenyl $\pi$ orbitals in the same binding energy range was observed in the PES spectra of $C_6H_5CO_2^-$ and other substituted benzene carboxylate anions.[52]

**4.5. Spectral Assignments of IV and V.** In **IV** and **V** (Figure 2), the S on the distal ligand is coordinated to one Fe atom, displacing the $CN^-$ ligand on the same Fe. Thus, although the oxidation state of the two Fe centers remains the same, the total charge of **IV** and **V** becomes −1. Consequently, the electron binding energies of **IV** and **V** are significantly increased by more than 3 eV (Figure 3). The X band of **IV** and **V** are nearly identical to those in **I**−**III**, suggesting that the Fe 3d orbitals are not significantly influenced. The A band of **IV** and **V**, however, showed significant changes compared to that in **I**−**III**. This band is due to detachment from the MOs of Fe−S bonding character. The additional S coordination in **IV** and **V** is expected to induce changes to the manifold of the Fe−S bonding orbitals. The relative intensity of the B band in **IV** and **V** decreased because now there is only one $CN^-$ ligand. Its broader width was likely due to the overlapping with detachment features of the S lone pairs.

## 5. Concluding Remarks

From the PES spectra and the qualitative assignments, we can conclude that the electronic structures of all of the five Fe(I)−Fe(I) model complexes **I**−**V** are very similar. The HOMO of these complexes is an Fe 3*d* orbital and all the Fe 3d derived MOs lie above the ligand-based MOs, giving rise to a "normal level scheme". This MO level pattern is quite different from those of ferredoxin-type [4Fe4S] and [2Fe2S] cluster complexes, which have the so-called "inverted level scheme"; that is, the majority spin levels of the Fe 3d derived MOs are below the S lone pairs due to the strong exchange splitting.[25−27] Unequivocally, the strong field ligands CO and $CN^-$ play a major role in determining the electronic structure of the di-iron active center in the [Fe]-hydrogenase. We also observed subtle differences in the PES spectra of the five model Fe(I)−Fe(I) complexes because of their slightly different ligands, reflecting the sensitivity of the electronic structure to the ligand environments in the di-iron complexes. It would be interesting to elucidate these differences in electronic structures among the five di-iron complexes using more advanced theoretical calculations. It should be mentioned that the ligand environments of the di-iron centers in these analogues are not exactly the same as the di-iron site in [Fe]-hydrogenase because of the absence of a bridging CO ligand. Both DFT calculations[23,24] and FTIR experiments[16] showed that the fully reduced Fe(I)−Fe(I) species favors the terminal CO conformation and a transient bridging CO intermediate can be generated by one-electron oxidation. It would be interesting to elucidate how the electronic structure of complexes with a bridged CO differs from those of **I**−**V**. Establishing the detailed electronic structure of the di-iron active site of the H-cluster is critical to an understanding of the mechanism of $H_2$ metabolism by the [Fe]-hydrogenases. The current PES spectra provide a first step toward defining the electronic structure of di-iron assemblies related to the H-center and offer a set of experimental results which may be valuable to further theoretical efforts.

**Acknowledgment.** Support of this work by the National Institutes of Health (GM-63555 to L.S.W.) and BBSRC (C.J.P.) and the John Innes Foundation (M.R.) is gratefully acknowledged. The experimental work done at Washington was performed at the W. R. Wiley Environmental Molecular Sciences Laboratory, a national scientific user facility sponsored by DOEs Office of Biological and Environmental Research and located at Pacific Northwest National Laboratory, which is operated for DOE by Battelle.

## References and Notes

(1) Adams, M. W. W. *Biochim. Biophys. Acta* **1990**, *1020*, 115.
(2) Adams, M. W. W.; Stiefel, E. I. *Science* **1998**, *282*, 1842.
(3) Albracht, S. P. J. *Biochim. Biophys. Acta* **1994**, *1118*, 167.
(4) Cammack, R. *Nature* **1999**, *397*, 214.
(5) Pierik, A. J.; Hulstein, M.; Hagen, W. R.; Albracht, S. P. J. *Eur. J. Biochem.* **1998**, *258*, 572.
(6) Van der Spek, T. M.; Arendsen, A. F.; Happe, R. P.; Yun, S.; Bagley, K. A.; Hagen, W. R.; Albracht, S. P. J. *Eur. J. Biochem.* **1996**, *237*, 629.
(7) Pierik, A. J.; Hagen, W. R.; Redeker, J. S.; Wlbert, R. B. G.; Boersma, M.; Verhagen, M. F. J. M.; Grande, H. J.; Veeger, C.; Mutsaers, P. H. A.; Sand, R. H.; Dunham, W. R. *Eur. J. Biochem.* **1992**, *209*, 63.
(8) Peters, J. W.; Lanzilotta, W. N.; Lemon, B. J.; Seefedt, L. C. *Science* **1998**, *282*, 1853.
(9) Nicolet, Y.; Piras, C.; Legrand, P.; Hatchikian, C. E.; Fontecilla-Camps, J. C. *Structure* **1999**, *7*, 13.
(10) Nicolet, Y.; Lemon, B. J.; Fontecilla-Camps, J. C.; Peters, J. W. *Trends Biochem. Sci*. **2000**, *25*, 138.
(11) deLacey, A. L.; Stadler, C.; Cavazza, C.; Hatchikian, E. C.; Fernandez, V. M. *J. Am. Chem. Soc*. **2000**, *122*, 11232.
(12) Nicolet, Y.; deLacey, A. L.; Vernede, X.; Fernandez, V. M.; Hatchikian, E. C.; Fontecilla-Camps, J. C. *J. Am. Chem. Soc*. **2001**, *123*, 1596.
(13) Popescu, C. V.; Münck, E. *J. Am. Chem. Soc*. **1999**, *121*, 7877.
(14) Cloirec, A. L.; Best, S. P.; Borg, S.; Davies, S. C.; Evans, D. J.; Hughes, D. L.; Pickett, C. J. *Chem. Commun*. **1999**, 2285.
(15) Razavet, M.; Davies, S. C.; Hughes, D. L.; Pickett, C. J. *Chem. Commun*. **2001**, 847.
(16) Razavet, M.; Borg, S. J.; George, S. J.; Best, S. P.; Fairhurst, S. A; Pickett, C. J. *Chem. Commun*. **2002**, 700.
(17) George, S. J.; Cui, Z.; Razavet, M.; Pickett, C. J. *Chem. Eur. J*. **2002**, *8*, 4037.
(18) Lyon, E. J.; Georgakaki, I. P.; Reibenspies, J. H.; Darensbourg, M. Y. *Angew. Chem., Int. Ed*. **1999**, *38*, 3178.

(19) Schmidt, M.; Contakes, S. M.; Rauchfuss, T. B. *J. Am. Chem. Soc*. **1999**, *121*, 9736.
(20) Li, H.; Rauchfuss, T. B. *J. Am. Chem. Soc*. **2002**, *124*, 726.
(21) Kaasjager, V. E.; Henderson, R. K.; Bouwman, E.; Lutz, M.; Spek, A. L.; Reedijk, J. *Angew. Chem., Int. Ed*. **1998**, *37*, 1668.
(22) Lwarence, J. D.; Rauchfuss, T. B.; Wilson, S. R. *Inorg. Chem*. **2002**, *41*, 6193.
(23) Cao, Z.; Hall, M. B. *J. Am. Chem. Soc*. **2001**, *123*, 3734.
(24) Liu, Z. P.; Hu, P. *J. Am. Chem. Soc*. **2002**, *124*, 5175.
(25) Noodleman, L.; Norman, J. G., Jr.; Osborne, J. H.; Aizman, A.; Case, D. A. *J. Am. Chem. Soc.* **1985**, *107*, 3418.
(26) Noodleman, L.; Case, D. A. *Adv. Inorg. Chem.* **1992**, *38*, 423.
(27) Noodleman, L.; Peng, C. Y.; Case, D. A.; Mouesca, J. M. *Coord. Chem. Rev*. **1995**, *144*, 199.
(28) Koerner, J. B.; Ichiye, T. *J. Phys. Chem. B* **1997**, *101*, 3633.
(29) Butcher, K. D.; Gebhard, M. S.; Solomon, E. I. *Inorg. Chem.* **1990**, *29*, 2067.
(30) Rose Williams, K.; Hedman, B.; Hodgson, K. O.; Solomon, E. I. *Inorg. Chim. Acta* **1997**, *263*, 315.
(31) Rose, K.; Shadle, S. E.; Eidsness, M. K.; Kurtz, D. M., Jr.; Scott, R. A.; Hedman, B.; Hodgson, K. O.; Solomon, E. I. *J. Am. Chem. Soc*. **1998**, *120*, 10743.
(32) Fan, H. J.; Hall, M. B. *J. Am. Chem. Soc.* **2001**, *123*, 3828. Liu, Z. P.; Hu, P. *J. Chem. Phys*. **2002**, *117*, 8177.
(33) Wang, L. S.; Ding, C. F.; Wang, X. B.; Barlow, S. E. *Rev. Sci. Instrum*. **1999**, *70*, 1957.
(34) Wang, L. S.; Wang, X. B. *J. Phys. Chem. A* **2000**, *104*, 1978.
(35) Wang, X. B.; Yang, X.; Wang, L. S. *Int. Rev. Phys. Chem*. **2002**, *21*, 473.
(36) Wang, X. B.; Wang, L. S. *J. Chem. Phys*. **2000**, *112*, 6959.
(37) Yang, X.; Wang, X. B.; Fu, Y. J.; Wang, L. S. *J. Phys. Chem. A* **2003**, *107*, 1703.
(38) Yang, X.; Wang, X. B.; Niu, S. Q.; Pickett, C. J.; Ichiye, T.; Wang, L. S. *Phys. Rev. Lett.* **2002**, *89*, 163401.
(39) Wang, X. B.; Ding, C. F.; Wang, L. S. *Phys. Rev. Lett*. **1998**, *81*, 3351.
(40) Wang, X. B.; Ding, C. F.; Wang, L. S. *Chem. Phys. Lett*. **1999**, *307*, 391.
(41) Wang, L. S.; Ding, C. F.; Wang, X. B.; Nicholas, J. B. *Phys. Rev. Lett.* **1998**, *81*, 2667.
(42) Wang, X. B.; Ferris, K.; Wang, L. S. *J. Phys. Chem. A* **2000**, *104*, 25.
(43) Butcher, C. P. G.; Johnson, B. F. G.; McIndoe, J. S.; Yang, X.; Wang, X. B.; Wang, L. S. *J. Chem. Phys*. **2002**, *116*, 6560.
(44) Wei, C. H.; Dahl, L. F. *Inorg. Chem*. **1965**, *4*, 1.
(45) Ginsburg, R. E.; Rothrock, R. K.; Finke, R. G.; Collman, J. P.; Dahl, L. F. *J. Am. Chem. Soc*. **1979**, *101*, 6550.
(46) Seyferth, D.; Henderson, R. S.; Song, L. C. *Organometallics* **1982**, *1*, 125.
(47) Teo, B. K.; Hall, M. B.; Fenske, R. F.; Dahl, L. F. *Inorg. Chem*. **1975**, *14*, 3103.
(48) Andersen, E. L.; Fehlner, T. P.; Foti, A. E.; Salahub, D. R. *J. Am. Chem. Soc*. **1980**, *102*, 7422.
(49) Dekock, R. L.; Baerends, E. J.; Hengelmolen, R. *Organometallics* **1984**, *3*, 289.
(50) Dam, H. V.; Louwen, J. N.; Oskam, A. *J. Electron Spectrosc. Relat. Phenom*. **1980**, *21*, 57.
(51) Bradforth, S. E.; Kim, E. H.; Arnold, D. W.; Neumark, D. M. *J. Chem. Phys*. **1993**, *98*, 800.
(52) Wang, X. B.; Nicholas, J. B.; Wang, L. S. *J. Chem. Phys*. **2000**, *113*, 653.